

## Dopamine precursor depletion impairs structure and efficiency of resting state brain functional networks



Felix Carbonell<sup>a</sup>, Atsuko Nagano-Saito<sup>a</sup>, Marco Leyton<sup>c</sup>, Paul Cisek<sup>b</sup>, Chawki Benkelfat<sup>c</sup>, Yong He<sup>d</sup>, Alain Dagher<sup>a,\*</sup>

<sup>a</sup> Montreal Neurological Institute, McGill University, Montreal, Canada

<sup>b</sup> Département de Physiologie, Université de Montréal, Montréal, Canada

<sup>c</sup> Department of Psychiatry, McGill University, Montreal, Canada

<sup>d</sup> State Key Laboratory of Cognitive Neuroscience and Learning, Beijing Normal University, Beijing, China

### ARTICLE INFO

#### Article history:

Received 14 May 2013

Received in revised form

20 December 2013

Accepted 30 December 2013

Available online 9 January 2014

#### Keywords:

Dopamine

Functional connectivity

Resting state

Small world network

Efficiency

Modularity

fMRI

Default mode network

### ABSTRACT

Spatial patterns of functional connectivity derived from resting brain activity may be used to elucidate the topological properties of brain networks. Such networks are amenable to study using graph theory, which shows that they possess small world properties and can be used to differentiate healthy subjects and patient populations. Of particular interest is the possibility that some of these differences are related to alterations in the dopamine system. To investigate the role of dopamine in the topological organization of brain networks at rest, we tested the effects of reducing dopamine synthesis in 13 healthy subjects undergoing functional magnetic resonance imaging. All subjects were scanned twice, in a resting state, following ingestion of one of two amino acid drinks in a randomized, double-blind manner. One drink was a nutritionally balanced amino acid mixture, and the other was tyrosine and phenylalanine deficient. Functional connectivity between 90 cortical and subcortical regions was estimated for each individual subject under each dopaminergic condition. The lowered dopamine state caused the following network changes: reduced global and local efficiency of the whole brain network, reduced regional efficiency in limbic areas, reduced modularity of brain networks, and greater connection between the normally anti-correlated task-positive and default-mode networks. We conclude that dopamine plays a role in maintaining the efficient small-world properties and high modularity of functional brain networks, and in segregating the task-positive and default-mode networks.

This article is part of the Special Issue Section entitled 'Neuroimaging in Neuropharmacology'.

© 2014 Elsevier Ltd. All rights reserved.

### 1. Introduction

The study of whole brain spontaneous neuronal activity has recently emerged as a tool to uncover the structure of large-scale brain networks. Regional measurements of slow (<0.1 Hz) spontaneous fluctuations in the blood oxygen level-dependent (BOLD) functional Magnetic Resonance Imaging (fMRI) signal disclose patterns of correlation that reveal functional neuronal networks (Biswal et al., 1995; Lowe et al., 1998; Greicius et al., 2003; Fox et al., 2005). Whole brain exploratory techniques (Kiviniemi et al., 2003; Beckmann et al., 2005; De Luca et al., 2006) and seed-based approaches (Lowe et al., 1998; Cordes et al., 2001) have been used for detecting functional connectivity on a voxel-wise basis. Region of

interest (ROI)-based analysis is a useful technique for describing functional connectivity within the framework of graph theory (Salvador et al., 2005; Achard et al., 2006; He et al., 2009b; Bullmore and Sporns, 2009). This approach is based on extracting averaged BOLD signals from a number of anatomically defined cortical and subcortical regions, computing a suitable correlation measure between every pair of ROI-averaged signals, and using graph theory to make inferences about the properties of the resulting neural networks.

Patterns in functional connectivity derived from spontaneous brain activity may be used for segregating healthy and patient populations (Fox and Raichle, 2007; Supekar et al., 2008; Liu et al., 2008), or for studying the effect of modulatory neurotransmitters, such as dopamine (Achard and Bullmore, 2007; Kelly et al., 2009a, 2009; Helmich et al., 2010). One motivation for focusing on the dopamine system is the number of psychiatric and neurological diseases (Honey et al., 2003; Honey and Bullmore, 2004) and the wide range of cognitive tasks (e.g. Nagano-Saito et al., 2008) in

\* Corresponding author. 3801 University St., Montreal, QC H3A 2b4, Canada. Tel./fax: +1 514 398 1726.

E-mail address: [alain.dagher@mcgill.ca](mailto:alain.dagher@mcgill.ca) (A. Dagher).

which it is implicated. Another motivation derives from studies showing that dopamine can affect spontaneous oscillations of basal ganglia neurons (Walters et al., 2000), as well as correlation of neuronal activity both within basal ganglia (Pessiglione et al., 2005) and between basal ganglia and cortex in animals (Costa et al., 2006) and humans (Meyer-Lindenberg et al., 2007; Nagano-Saito et al., 2008). These studies suggest that large-scale networks that involve basal ganglia could be disrupted by alterations in dopamine function.

The aim of the current study was to investigate the effects of lowered dopamine transmission on resting state functional connectivity of healthy subjects, assessed using graph theory. We used the acute phenylalanine/tyrosine depletion (APTD) technique, which decreases dopamine synthesis and reduces both baseline dopamine levels and stimulated dopamine release in humans (Montgomery et al., 2003; Leyton et al., 2004). Our previous fMRI studies used the APTD technique to detect dopamine-related changes in activation and/or connectivity during specific cognitive tasks (Nagano-Saito et al., 2008, 2012; Coull et al., 2012). In contrast, we use here a ROI-based approach to study how dopamine depletion impairs functional connectivity, network efficiency and modularity by using BOLD signals collected during the resting state.

## 2. Materials and methods

### 2.1. Subjects

Seventeen healthy right-handed subjects (mean age,  $23.6 \pm 4.4$  years; range, 19–34, eleven males) participated in this study, however three (one male and two females) had to be eliminated from the final analysis because one fell asleep during scanning, and two regurgitated the amino acid drink. One data set was removed for excessive motion, leaving a total of 13 subjects. No subject had a history of neurologic psychiatric disorder. Only non-smokers and social smokers (less than 5 cigarettes per day) participated. All subjects gave informed consent to the protocol, which was reviewed and approved by the Research Ethics Boards of the Montreal Neurological Institute.

### 2.2. Dopamine depletion

The acute dopamine precursor depletion technique has been previously described by Leyton et al. (2000). Subjects were tested twice, on separate days at least 3 days apart. The day before each test session, subjects ate a low-protein diet provided by the investigators and fasted from midnight. On the test days, subjects arrived at 9:00 A.M. and had blood samples drawn to measure plasma amino acid concentrations (Leyton et al., 2000). They then ingested one of two amino acid drinks in a randomized, double-blind manner. One drink was a nutritionally balanced 100 g amino acid mixture (BAL), and the other was tyrosine and phenylalanine deficient (APTD) but otherwise identical. Eight subjects received BAL on the first day, and nine subjects received APTD first. After ingestion of the amino acid drink, around 9:40 A.M., subjects remained awake in a quiet room before performing simple reaction time tasks, which started at 12:30 P.M. in the same room. This was followed by functional magnetic resonance imaging (fMRI) starting at 1:30 P.M. At the end of the fMRI test session, at 3:00 P.M., subjects had a second blood sample drawn to measure plasma amino acid concentration.

### 2.3. Data acquisition and preprocessing

Subjects were scanned at the Montreal Neurological Institute (MNI) using a 3T Siemens (Erlangen, Germany) Magnetom Trio MRI scanner. The study consisted of acquisition of two sets of echoplanar T2\*-weighted images with blood oxygenation level-dependent (BOLD) contrast (echo time, 30 ms; flip angle,  $90^\circ$ ) and a high-resolution, T1-weighted, three-dimensional volume acquisition for anatomical localization (1 mm<sup>3</sup> voxel size). Only the first set of BOLD acquisitions was used in this study. The second set consisted of a cognitive task described elsewhere (Nagano-Saito et al., 2012). The first acquisition comprised the resting state fMRI. Each participant was asked to lie quietly at rest with eyes closed during acquisition. One hundred and seventy seven whole brain volumes were acquired continuously every 2.04s for a total of 361s. Volumes contained 35 slices of 4 mm thickness (matrix size,  $64 \times 64$  pixels; voxel size,  $4 \times 4 \times 4$  mm<sup>3</sup>). The data were pre-processed using the standard-stereotaxic fMRI preprocessing pipeline implemented in the neuroimaging analysis kit (NIAC, Bellec et al., 2012). The first 5 volumes of each run were discarded to minimize saturation effects. Each dataset was corrected for interslice difference in acquisition time and rigid body motion. The whole dataset was then submitted to the CORSICA procedure (Perlberg et al., 2007) for removal of structured physiological noise, and a band pass filter was applied in the range [0.01–

0.1] Hz. For each subject, the mean motion-corrected time-averaged functional volume was co-registered with the individual T1 scan (Collins et al., 1994), which was in turn non-linearly transformed to the Montreal Neurological Institute (MNI) non-linear template using the CIVET pipeline (Zijdenbos et al., 2002). The functional volumes were re-sampled in MNI space at 2 mm isotropic resolution and not spatially smoothed before regional parcellation of each cerebral hemisphere into 45 anatomical regions of interest (Supplementary Table S1), according to the Automatic Anatomical Labelling atlas (Tzourio-Mazoyer et al., 2002).

### 2.4. Statistical analysis of functional networks

For each voxel time course (BOLD data) we use a resting state version of the model proposed in Worsley et al. (2002) and implemented in the fMRIStat package (<http://www.math.mcgill.ca/keith/fmristat/>):

$$\text{BOLD}(t) = \text{Confounds}(t) + \text{LinearDrift}(t) + e(t), \quad (1)$$

where  $\text{Confounds}(t)$  represents the matrix of the six parameters resulting from the rigid body motion correction, the average white matter and the average cerebrospinal fluid time courses.  $\text{LinearDrift}(t)$  is a linear polynomial for reducing variance due to temporal linear trend in the BOLD signal, and the error  $e(t)$  was modeled as an order-8 auto-regressive process (AR(8) model) (see Discussion). The residuals of this regression constituted the time series employed in the ROI-based connectivity analysis. Regional mean time series were calculated for each subject by averaging the fMRI time series over all voxels in each of the 90 parcellated anatomical regions. For each individual data set, the Pearson correlation coefficient was estimated between each pair of the 90 mean time series, resulting in a symmetric  $90 \times 90$  correlation matrix.

Then, for each of the two conditions (BAL and APTD) we computed a common (group-based)  $90 \times 90$  correlation matrix  $R$  based on a random effects model over the individual functional networks (Field, 2001). Each individual correlation matrix  $R_j^i$  was converted to a standard normal metric by means of the Fischer r-to-Z transformation:

$$Z_j^i = \frac{1}{2} \log \left( \frac{1 + R_j^i}{1 - R_j^i} \right),$$

where  $R_j^i$  denote the individual correlation matrices for condition  $i = 1, 2$  ( $i = 1 = \text{BAL}$  and  $i = 2 = \text{APTD}$ ) and subject  $j = 1, \dots, N_{\text{Sub}}$ . According to the properties of the Fischer r-to-Z transformation, each  $Z_j^i$  is approximately normally distributed with zero mean and variance equal to  $1/(df-3)$ , where  $df$  are the residual degrees of freedom of the model. Indeed, having approximately Gaussian distributions facilitates the between-condition comparisons of correlation matrices under the framework of the General Linear Model.

The transformed correlation matrices  $Z_j^i$  were then used to generate a weighted average (group-based)  $\bar{Z}$  in which each individual  $Z_j^i$  is weighted by the inverse of the corresponding individual adjusted variances  $w_{\text{rand}}^i$  (Field, 2001):

$$\bar{Z} = \frac{\sum_{j=1}^{N_{\text{Sub}}} \frac{Z_j^i}{w_{\text{rand}}^i}}{\sum_{j=1}^{N_{\text{Sub}}} \frac{1}{w_{\text{rand}}^i}} = \frac{\sum_{j=1}^{N_{\text{Sub}}} Z_j^i}{N_{\text{Sub}}}.$$

Here, each individual adjusted variance is given by the sum of a within-subject variance component  $1/(df-3)$  and a between-subject variance component  $\tau_i^2$ . That is,  $w_j^i = 1/(df-3) + \tau_i^2$ , with  $\tau_i^2 = (1 - N_{\text{Sub}} + (df-3) \sum_{j=1}^{N_{\text{Sub}}} (Z_j^i - \bar{Z}^i)^2) / (df-3)(N_{\text{Sub}} - 1)$ . In this way, we have generated a random effects model to define the adjusted individual variance of the Z-transformed variables  $Z_j^i$ . Thus, in contrast to classical fixed effects modeling (variance =  $1/(df-3)$ ), the adjusted variance term includes an additional between-subjects variance component. This typically yields more conservative tests for group-based statistics (Field, 2001).

Finally, in order to define group-based correlation matrices, the average matrices  $\bar{Z}$  were converted back to r-scale by the Z-to-r transformation  $R^i = (e^{2\bar{Z}} - 1) / (e^{2\bar{Z}} + 1)$  (Field, 2001).

The statistical comparison between the two conditions was carried out by using a paired  $T$  test over the whitened (adjusted variance-corrected) variables  $Z_j^i / \sqrt{w_{\text{rand}}^i}$ . This  $T$  test was implemented within a General Mixed-Effects Linear Model, which allowed us to consider individual differences in variances as well as to remove sex and age effects as modeled covariates. Our implementation of the general mixed-effects model uses the restricted maximum likelihood (REML) estimation method (Pinheiro and Bates, 2000). In particular, we employed the Matlab code provided in the SurfStat toolbox (<http://www.math.mcgill.ca/keith/surfstat/>) (Worsley et al., 2009). In order to detect significant differences in correlation patterns between the two conditions (BAL and APTD), the resulting  $T$  Statistical Parametric Map (SPM) was submitted to a False Discovery Rate (FDR) (Benjamini and Yekutieli, 2001) thresholding criterion to account for multiple comparisons.

### 2.5. Network properties

We computed network efficiency measures to quantify the small-world behavior of our functional brain networks (Latora and Marchiori, 2001). These measures are indicative of how efficiently information can be propagated over the network (Achard and Bullmore, 2007) and can be evaluated at different network scales to yield global, local and regional efficiency. These measures have a number of conceptual and technical advantages compared to the standard small-world parameters (characteristic path length ( $L$ ) and clustering coefficient ( $C$ )) (Latora and Marchiori, 2001). Indeed, the quantities  $1/L$  and  $C$  can be seen as first approximations of network efficiency, evaluated at global and local scale, respectively (Latora and Marchiori, 2001).

Suppose that an  $N$ -dimensional correlation matrix  $\mathbf{R}$  has been thresholded at a value  $r$  to create an adjacency matrix  $\mathbf{A}$ , where the entry  $a_{ij}$  of  $\mathbf{A}$  is defined as either 1, if  $|R_{ij}| > r$ , or 0 otherwise. This adjacency matrix defines an unweighted graph (network)  $G$  comprising  $N$  nodes, connected by undirected edges corresponding to the nonzero entries of  $\mathbf{A}$ . Then, for such a graph  $G$ , the wiring cost  $K$  is defined as the ratio between the number of edges in the graph and the total number of possible edges (i.e.  $N(N-1)/2$ ). Notice that, for each node, one can also compute the nodal contribution to the wiring cost value as the ratio between the actual number of edges connected to that node and the total number of possible edges. More generally, for any pre-defined two subsets of nodes, one can also compute the wiring cost contribution of their interaction by taking the ratio between the number of edges connecting the two subsets and the total number of possible edges in the network.

The global efficiency  $E_{\text{glob}}$  is defined as in Latora and Marchiori (2001):

$$E_{\text{glob}}(G) = \frac{1}{N(N-1)} \sum_{i \neq j \in G} \frac{1}{d_{ij}},$$

where  $d_{ij}$  is the shortest path length between nodes  $i$  and  $j$  in  $G$ . The local efficiency  $E_{\text{loc}}$  is calculated as (Latora and Marchiori, 2001):

$$E_{\text{loc}}(G) = \frac{1}{N} \sum_{i \in G} E_{\text{glob}}(G_i),$$

where  $G_i$  denotes the sub-graph of the neighbors of node  $i$ . Note that path length refers to the number of edges between two nodes and not to physical distance.

A small world network is one with  $E_{\text{glob}}$  less than a random graph but greater than a regular lattice and  $E_{\text{loc}}$  greater than a comparable random graph (Watts and Strogatz, 1998; Achard and Bullmore, 2007). Here, the comparable random networks were generated according to the random re-wiring procedure described in Maslov and Sneppen (2002). In particular, we retained the degree of each node during the rewiring process such that the degree distribution of the entire network is preserved. For comparison purposes, we generated 100 of these random networks per subject and dopaminergic condition and calculated their mean  $E_{\text{glob}}$  and  $E_{\text{loc}}$  as described earlier.

Two different measures were used here for determining the relative importance of each node within the network: regional efficiency and betweenness. The regional efficiency  $E_{\text{reg}}$  for a given node  $i$  is defined as (Achard and Bullmore, 2007):

$$E_{\text{reg}}(i) = \frac{1}{N-1} \sum_{i \neq j \in G} \frac{1}{d_{ij}}.$$

Regional efficiency is therefore a measure of each node's connectedness with every other node. A node with high regional efficiency can be called a hub. Betweenness is a centrality measure that detects those nodes with high occurrence on the shortest paths between other nodes, which is defined as (Freeman, 1977):

$$B(i) = \frac{2}{(N-1)(N-2)} \sum_{\substack{j \neq i \neq k \in G \\ j \neq k}} \frac{\sigma_{jk}(i)}{\sigma_{jk}},$$

where  $\sigma_{jk}$  denotes the number of shortest paths from  $j$  to  $k$ , and  $\sigma_{jk}(i)$  is the number of shortest paths from  $j$  to  $k$  that pass through node  $i$ .

As discussed below, the choice of the correlation threshold  $r$  has a major impact on the adjacency matrix  $\mathbf{A}$ . A common approach is to threshold the correlation matrix in order to achieve a desired wiring cost value  $K$ , which is equal to the total number of edges in the graph divided by the maximum number of edges (He et al., 2009a). This allows analysis over the entire range of cost values  $[0, 1]$  and yields definitions of integrated efficiency measures. Hence, we define the integrated regional efficiency for node  $i$  over the cost interval  $[K_1, K_2] \subset [0, 1]$  as

$$\frac{\int_{K_1}^{K_2} E_{\text{reg}}(i, K) dK}{K_2 - K_1},$$

where the term  $E_{\text{reg}}(i, K)$  means that regional efficiency has been considered as a function of the wiring cost  $K$ . In a similar way we can define integrated measures of global efficiency, local efficiency and betweenness. Integrated measures serve to

summarize network behavior over a particular cost interval, for instance, the interval over which the network satisfies the small-world property.

For each cost value in the range  $[0, 1]$  we used a paired  $t$ -test for the comparison of the values  $\log(E_{\text{glob}}^1/1 - E_{\text{glob}}^1)$  and  $\log(E_{\text{glob}}^2/1 - E_{\text{glob}}^2)$ ,  $j = 1, \dots, N_{\text{Subj}}$ , where for each  $j$ ,  $E_{\text{glob}}^1$  and  $E_{\text{glob}}^2$  represent either any of the efficiency parameters  $E_{\text{glob}}$ ,  $E_{\text{loc}}$  or  $E_{\text{reg}}$  corresponding to the BAL and APTD conditions, respectively. Note that we used a logit model due to the efficiency parameters' values varying between 0 and 1. FDR (Benjamini and Yekutieli, 2001) thresholding was employed to account for multiple comparisons over the interval  $[0, 1]$ .

### 2.6. Modular organization

Another important network property is modularity (Newman and Girvan, 2004). It has been shown that fMRI resting state networks have an intrinsic modular organization. By definition, the number of connections within modules is greater than the expected number of connections in an equivalent network with edges placed at random (Meunier et al., 2009; He et al., 2009b). The modularity  $Q(G)$  for a network partition  $G = \{G_1, \dots, G_M\}$  into  $M$  modules is given by (Newman and Girvan, 2004):

$$Q(G) = \sum_{i=1}^M \frac{2e_i}{N(N-1)} - \left( \frac{d_i}{N(N-1)} \right)^2,$$

where  $e_i$  denotes the number of edges between nodes in module  $i$  and  $d_i$  is the sum of the degrees of all nodes in module  $i$ . The module identification process consists in finding a partition that maximizes the modularity function  $Q(G)$ . Several algorithms have been developed for this purpose (see Fortunato (2010) for a review). Here, we followed the spectral bisection algorithm as proposed by Newman (2006). The spectral bisection algorithm has been shown to produce better results than other competitive methods with shorter computational times (Newman, 2006). However, it has been recently shown (Good et al., 2010) that the modularity function  $Q(G)$  typically admits an exponential number of distinct high scoring sub-optimal solutions and usually lacks a clear global maximum (optimal solution). We address this issue by employing an additional fine-tuning approach (Newman, 2006), which consists of a greedy strategy based on iterative re-distribution of each single node from a module to either another existing module or to a new module in order to minimize the modularity function in each re-allocation.

In this way, meaningful modular partitions can be obtained for both individual and group-based functional networks. An important concern is the stability of the resulting group-based modular partitions. A bootstrapping approach has been recently suggested for identifying stable functional modules produced by hierarchical clustering techniques (Bellec et al., 2010). Here we followed a similar approach for constructing stable group-based modular partitions. For each dopaminergic condition, we generated  $B = 500$  bootstrapped group-based correlation matrices. To generate each matrix we replaced individual matrices with randomly chosen matrices from the set of all individual correlation matrices and calculated the corresponding group-based correlation matrix. We then calculated the modular partitions for each of these 500 bootstrapped group-based correlation matrices and selected that modular partition achieving the maximal modularity value.

Finally, we used a permutation test for the statistical comparison of the group-based modular partitions corresponding to each dopaminergic condition. This approach requires a measure of similarity or agreement between any pair of modular partitions (either group-based or individual partitions). Here, we followed an information theoretic approach, by using the concept of normalized variation of information (Karrer et al., 2008) in order to define a distance measure between network partitions (see Appendix). Then, the normalized variation of information was used as the statistic of interest for the following permutation test. The permutation test was designed to determine whether the observed difference between the two group-based modular partitions was large enough to reject the null hypothesis that the two dopaminergic conditions produce identical modular partitions. A random permutation is created by switching the condition labels BAL and APTD for a random number of subjects. For each of 1000 such permutations, we calculated the group-based correlation coefficients for each randomized sample and computed the corresponding modular decompositions. Then the set of the corresponding 1000 normalized variation of information differences were taken as the approximate distribution of all possible differences under the null hypothesis that the modular partition is not determined by the dopaminergic condition. A  $p$ -value was then calculated based on the proportion of random permutations where the normalized variation of information was greater or equal to the actual difference observed between the two group-based modular partitions.

## 3. Results

### 3.1. Tyrosine depletion

APTD reduced the plasma concentration of amino acid precursors of dopamine. On arrival at the lab plasma tyrosine levels

were 52.5 (SD: 11.5) and 54.6 (12.2) micromol/l on BAL and APTD days, respectively. After fMRI scanning, they were 128.4 (42.3) and 11.1 (3.5) micromol/l, respectively. For phenylalanine, the initial levels were 48.1 (9.1) and 50.2 (6.4) micromol/l for BAL and APTD, respectively, and 78.6 (38.2) and 9.4 (3.3) micromol/l, respectively, after the fMRI sessions. Repeated-measures ANOVA indicated a significant condition difference between BAL and APTD and a condition by time interaction for both tyrosine and phenylalanine (all  $p < 0.001$ ).

The ratio of plasma tyrosine to large neutral amino acids, a measure of brain tyrosine availability, was unchanged during the BAL session (mean  $\pm$  SD:  $0.103 \pm 0.008$  before drinking the solution,  $0.100 \pm 0.03$  after scanning, 3% change,  $P = 0.67$ ) but reduced significantly after APTD ( $0.107 \pm 0.02$  before drinking the solution,  $0.008 \pm 0.004$  after scanning, 92% reduction,  $p < 0.0001$ ).

### 3.2. Functional connectivity

The common (group-based) functional connectivity network was computed for each dopaminergic condition (BAL and APTD). Both networks are shown as  $90 \times 90$  correlation matrices in the top row of Fig. 1. The 90 ROIs (left and right hemispheres of 45 anatomical regions) were arranged according to the anatomical organization presented in Supplementary Table S1. In this Table, each ROI was allocated to one of six pre-defined modules (frontal lobe, limbic lobe, occipital lobe, parietal lobe, temporal lobe and sub-cortical areas). Here, a module was defined as the set of ROIs that belong to the same pre-defined anatomical region.

For both conditions, we observed a markedly bilateral symmetry in the resulting connectivity network such that many of the strongest links in each network correspond to connections between contra-lateral homologous regions. This is evidenced as high correlation values on the 2nd diagonal (diagonal just above the

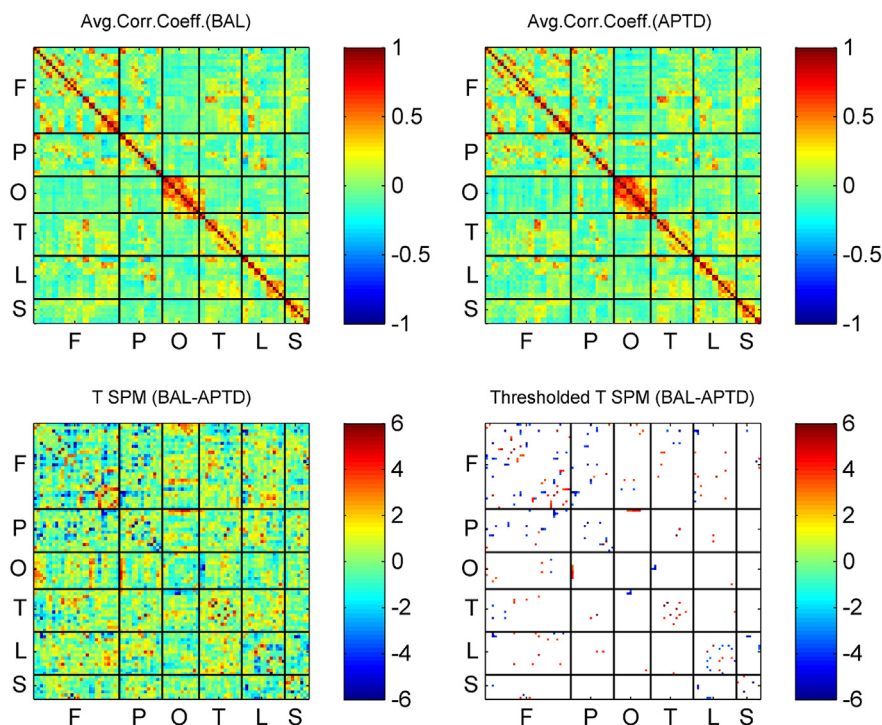
main diagonal) of the group-based correlation matrices. We can also observe that the occipital cortex is a region of dense local connectivity whereas the strongest long range connections are evident between the frontal lobe and the temporal and parietal lobes.

Fig. 1 also shows the  $T$  SPM corresponding to the null hypothesis of no differences in correlation between the two dopaminergic conditions. Significant pairs of correlations were obtained by thresholding the  $T$  SPM at FDR threshold  $t = 3.301$  ( $\alpha = 0.05$ ). Significant positive  $T$  values (in red) identify pairs of regions showing greater correlation strength in the BAL condition relative to APTD.

Table 1 shows the distribution of all statistically significant differences between BAL and APTD, according to the modular decomposition provided in Supplementary Table 1. The diagonal/off diagonal entries of this table correspond to the percent (relative to all statistically significant  $T$ 's) of significant  $T$ 's found within/between modules.

The greatest significant positive (BAL > APTD) differences (14%) correspond to short-range correlations within the frontal lobe. Another 7% of the significant positive  $T$  values correspond to correlations between regions in the frontal lobe and the limbic lobe. A number of significant positive  $T$  values also correspond to intra-lobe connections within temporal (4%) and limbic lobes (2.5%). Some other significant positive differences correspond to occipital–parietal (4%), frontal–occipital (5%) and frontal–temporal connections (3%).

In contrast, significant negative  $T$  values (blue color in Fig. 1) are associated with greater correlation in the APTD condition. The more evident significant negative  $T$  values correspond to connections within the frontal lobe (13.5%) and frontal–parietal (13%) connections. The limbic lobe also produced many significant differences (APTD > BAL). Indeed, intra limbic lobe connections



**Fig. 1.** Top row: Group-based correlation matrices for conditions BAL and APTD. There is strong network symmetry for both conditions. The occipital cortex and parietal cortex are regions of dense local connectivity while long-range connections are found between frontal cortex and lateral-temporal and parietal cortex. Bottom row: Statistical  $t$  SPM for differences in correlations between conditions BAL and APTD and anatomical classification of the significant values. The  $t$  map was thresholded at FDR level  $t = 3.301$  ( $\alpha = 0.05$ ). Highest positive  $t$  values (BAL > APTD) correspond to short-range connections among regions within the frontal lobe and between regions connecting frontal and temporal lobes. The most significant negative  $t$  values (APTD > BAL) correspond to connections within the default mode network.

**Table 1**

Distribution of all statistically significant connectivity differences between BAL and APTD. BAL condition increases the strength of short-range connections within frontal lobe as well as frontal–limbic connections. APTD also increases some frontal lobe connections as well as frontal–parietal connections. APTD-related connectivity enhancement was also seen in the limbic lobe. A detailed view of the significant negative differences (APTD > BAL) revealed that most of them correspond to connections within the Default Mode Network.

Region	Frontal	Parietal	Occipital	Temporal	Limbic	Sub-cortical
<b>Differences in connections (%) BAL &gt; APTD</b>						
Frontal	14.3	1.6	4.8	3.2	7.1	1.6
Parietal		0.8	4.0	1.6	1.6	0.0
Occipital			0.0	0.0	0.8	0.0
Temporal				4.0	1.6	0.0
Limbic					2.4	0.0
Sub-Cortical						0.8
<b>Differences in connections (%) BAL &lt; APTD</b>						
Frontal	13.5	12.7	1.6	3.2	4.0	1.6
Parietal		3.2	0.0	0.0	0.0	0.0
Occipital			0.0	2.4	0.0	0.0
Temporal				0.0	0.0	0.0
Limbic					4.0	3.2
Sub-cortical						0.8

produced 4% of all significant differences while another 4% and 3% of differences corresponded to frontal–limbic and subcortical–limbic connections, respectively. A more detailed view of these significant differences (APTD > BAL) revealed that most of them correspond to connections within a set of regions that includes the medial prefrontal cortex, left inferior parietal lobule, dorsal cingulate gyrus, posterior cingulate gyrus and precuneus. This set of regions is commonly referred to as the Default Mode Network (DMN) (Raichle et al., 2001; Greicius et al., 2003) because they routinely exhibit greater activity during the resting state than during performance of attention-demanding cognitive tasks. There

were also an additional number of connections showing significantly greater correlations in APTD than in BAL between regions belonging to the DMN and a set of regions commonly referred to as the Task Positive Network (TPN) (Fox et al., 2005, 2006). In contrast to the DMN, the TPN is a network of regions exhibiting activity increases during performance of attention-demanding cognitive tasks and includes areas such as fusiform gyrus, inferior occipital gyrus, lateral frontal cortex, lingual gyrus, cuneus, calcarine cortex and supplementary motor area. Finally, it is worth mentioning that a few significant negative differences (APTD > BAL) were also found among pairs of regions within the TPN.

### 3.3. Network analysis

The global and local efficiencies were calculated for each functional network in both dopaminergic conditions at all cost values in the interval  $K = [0, 1]$ . As expected, for  $K = 1$  both networks are fully connected, while, as  $K$  decreases towards 0, the networks become sparser.

Similarly, for each cost value, a corresponding random network with the same node degree and number of edges was generated for each network. Fig. 2 shows, for both conditions, the average global and local efficiency (across subjects) as a function of cost.

Note that the small world regime is observed in the interval  $K = [0.05, 0.3]$ . That is, for cost values in the range  $K = [0.05, 0.3]$ , both networks show global efficiency values smaller than the corresponding random network and local efficiency values greater than the random one. Importantly, in the cost range corresponding to a small world regime, the efficiency values are greater in the BAL condition than in the APTD condition. This is evidenced in the bottom panels of Fig. 2, which show the FDR-corrected  $p$ -values resulting from the statistical comparison of the BAL versus APTD difference for global and local efficiency, respectively, versus cost.

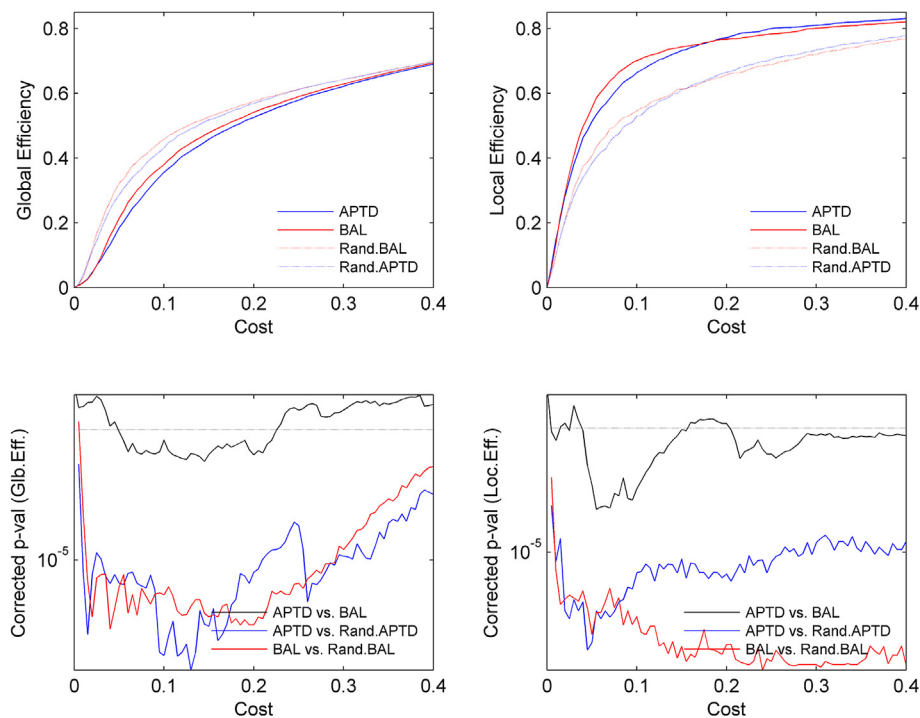


**Fig. 2.** Top row: Group average of local and global efficiencies for each condition as a function of wiring cost. A small world regime is evident in the wiring cost range  $[0.05, 0.3]$ . Both local and global efficiencies are greater in the BAL condition than in the APTD condition over the small-world range of wiring costs. Bottom row:  $p$ -value associated to a  $T$  test for differences in efficiency between conditions BAL and APTD. Significant statistical differences in global efficiency and local efficiency were found in the wiring cost intervals  $[0.055, 0.225]$ , and  $[0.04, 0.13]$ , respectively. See Supplementary Fig. 2 for similar plots with correlation rather than cost as the threshold criterion.

**Table 2**

T and corresponding *p*-values of regions showing statistically significant differences in regional efficiency and betweenness. Positive *t* values indicate a greater effect in BAL compared to APTD. Abbreviations: IFGoperc: inferior frontal gyrus (opercular), AMYG: amygdala, ORBmid: Orbitofrontal cortex (middle), ORBsupmed: orbitofrontal cortex (superior medial), PCUN: precuneus, MFG: middle frontal gyrus, ORBsup: orbitofrontal cortex (superior), ITG: inferior temporal gyrus, L: left, R: right.

Regional efficiency			Betweenness		
Region	<i>T</i>	<i>p</i>	Region	<i>T</i>	<i>p</i>
IFGoperc_R	5.113	0.0001	ITG_R	-2.835	0.0075
AMYG_R	2.821	0.0077	IFGoperc_R	2.187	0.0246
ORBmid_R	2.593	0.0117	ORBmid_R	1.895	0.0412
ORBsupmed_R	2.162	0.0257	ORBsupmed_R	1.806	0.0481
PCUN_R	2.152	0.0262			
MFG_R	2.042	0.0366			
ORBsup_L	1.943	0.0379			

These significant statistical differences in global and local efficiency were found in the cost intervals  $K = [0.055, 0.225]$  and  $K = [0.04, 0.13]$ , respectively. At no cost value was either efficiency measure greater in APTD than BAL. The integrated global efficiency in cost interval  $K = [0.055, 0.225]$  was of 0.444 and 0.420 for BAL and APTD conditions, respectively. Analogously, values for the integrated local efficiency in cost interval  $K = [0.04, 0.13]$  were of 0.648 and 0.611, respectively.

The regional efficiency and betweenness of each region were calculated for each individual functional network in both dopaminergic conditions and all cost values in the interval  $K = [0, 1]$ . Table 2 shows regions with the strongest differences in integrated regional efficiency and integrated betweenness for the small-world cost range  $K = [0.05, 0.3]$  (see abbreviations in Supplementary Table S1). Several regions belonging to the limbic system (orbitofrontal cortex, amygdala) show higher regional efficiency in the BAL condition than in the APTD condition. The overall connectivity of these regions with all other brain areas is reduced in the low dopamine

state. No regions showed greater regional efficiency in APTD. Only the right inferior temporal gyrus showed greater betweenness in APTD.

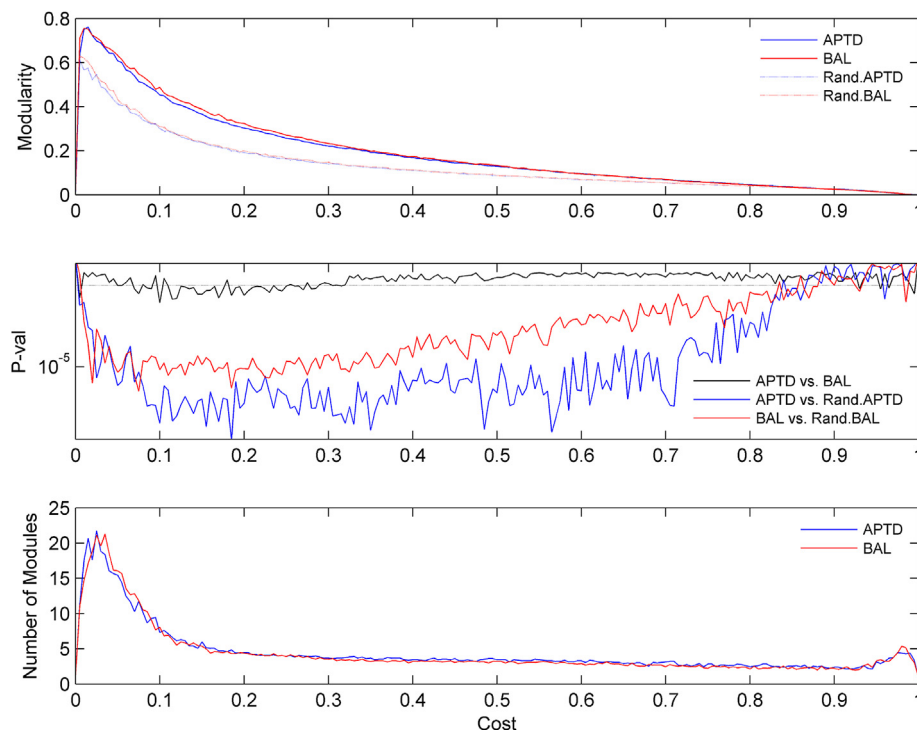
### 3.4. Modularity analysis

The modularity of each individual functional network was calculated for both dopaminergic conditions at all cost values  $K = [0, 1]$ . Fig. 3 shows the average modularity values across subjects.

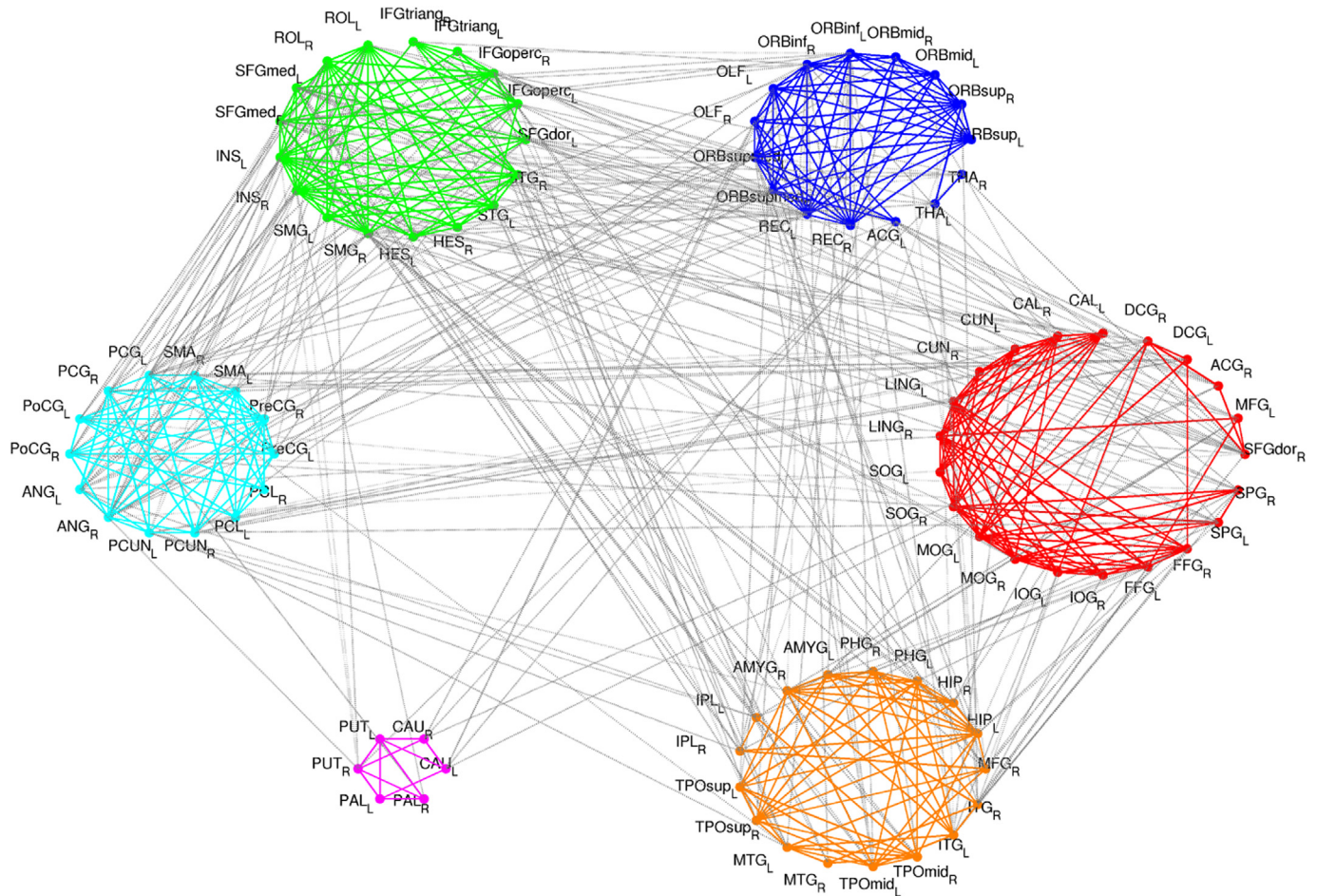
For both dopaminergic conditions, the resulting modularity values are higher than the values expected for the corresponding random networks, revealing a modular organization of brain networks. However, a higher modular functional organization is achieved for the BAL condition, which is corroborated by the FDR-corrected *p*-values resulting from the statistical comparison. This result indicates that the low dopamine state disrupts the modular organization of the brain at rest. The average number of modules resulting from the modular decomposition of each network is also shown in Fig. 3. Note that despite significantly higher modularity values in the BAL condition, no statistical differences were found between the numbers of modules produced in each condition; although there was a trend towards a greater number of modules in BAL (see below).

Fig. 4 represents the modular decomposition corresponding to group-based network in the BAL condition at cost value  $K = 0.15$ , which is a representative (midpoint) wiring cost value of the small world regime. Each color corresponds to a different module in the network. Edges within a module are plotted with the color of the module, while edges between modules are plotted in gray.

This modular decomposition produced 6 different modules with the following distribution (modularity score,  $Q = 0.48$ ). Module I (red) comprises 21 regions mostly from bilateral occipital lobe as well as a few regions from frontal, temporal and parietal lobe.



**Fig. 3.** Average of the population modularity for each condition BAL and APTD and *p*-value for the test corresponding to the difference in modularity between conditions. Higher modularity values are present in the BAL condition.



**Fig. 4.** Anatomical representation of the modularity analysis for the group-based connectivity network in the BAL condition at wiring cost  $K = 0.15$ . Nodes in each of the modules and edges within them are plotted with a single color, while edges between modules are plotted in black. Abbreviations in the [Supplementary Table](#). (For interpretation of the references to color in this figure legend, the reader is referred to the web version of this article.)

Module II (blue) is composed of 15 regions mostly from frontal lobe. Module III (green) includes 17 regions such as Heschl's gyrus, the insula, the superior temporal gyrus, the supramarginal gyrus and regions from the inferior frontal lobe. Module IV (cyan) contains 14 regions and includes the precentral and postcentral gyrus as well as the paracentral lobule, the supplementary motor area, the angular gyrus and the precuneus. Module V (magenta) consists of the basal ganglia: caudate, putamen and globus pallidus. Finally, Module VI (orange) contains 17 regions including the hippocampus, parahippocampal gyrus, amygdala and middle/superior temporal pole. A modular decomposition (modularity score,  $Q = 0.47$ ) was also carried out for the group-based functional network corresponding to the APTD condition at  $K = 0.15$ . This analysis produced only 5 modules (Fig. 5) although their composition was different from the one obtained for the BAL condition. The most evident difference consisted in assigning regions from the basal ganglia subnetwork (Module V in BAL condition) to different modules. Additionally, it seems that most of the regions corresponding to former Module VI in BAL condition are now split; some regions formed a single module (Module V, in magenta) in APTD condition, while the other regions were re-allocated to different modules. In short, APTD appeared to disrupt the integrity of the basal ganglia and limbic modules. Also, auditory and motor regions formed a single module in the APTD condition (cyan in Fig. 5).

The differences observed between the compositions of modules in the two dopaminergic conditions did not reach statistical

significance at  $\alpha = 0.05$ . The normalized variation of information between the two group-based modular partitions was equal to 0.33, which corresponds to a p-val of 0.09 when performing a permutation test.

## 4. Discussion

### 4.1. Alterations in functional connectivity

We describe four main effects of lowered dopamine synthesis on resting state brain networks. First, dopamine precursor depletion reduced short-range connections within frontal lobe and reduced connectivity between frontal lobe and posterior association areas. Dopamine precursor depletion also augmented connectivity between the DMN and the TPN. Second, the low dopamine state decreased the global and local efficiency of brain networks, within a range of costs compatible with small-world topology. Third, dopamine depletion reduced regional efficiency within the limbic system (amygdala and orbitofrontal cortex). Finally, lowered dopamine reduced brain modularity, dispersed the basal ganglia module that is normally present at rest, reassigning its component regions to other modules, and caused auditory and motor networks to become a single module.

The tyrosine depletion treatment used here transiently decreases dopamine synthesis (Palmour et al., 1998; McTavish et al., 1999b; Leyton et al., 2000) and reduces baseline (tonic)

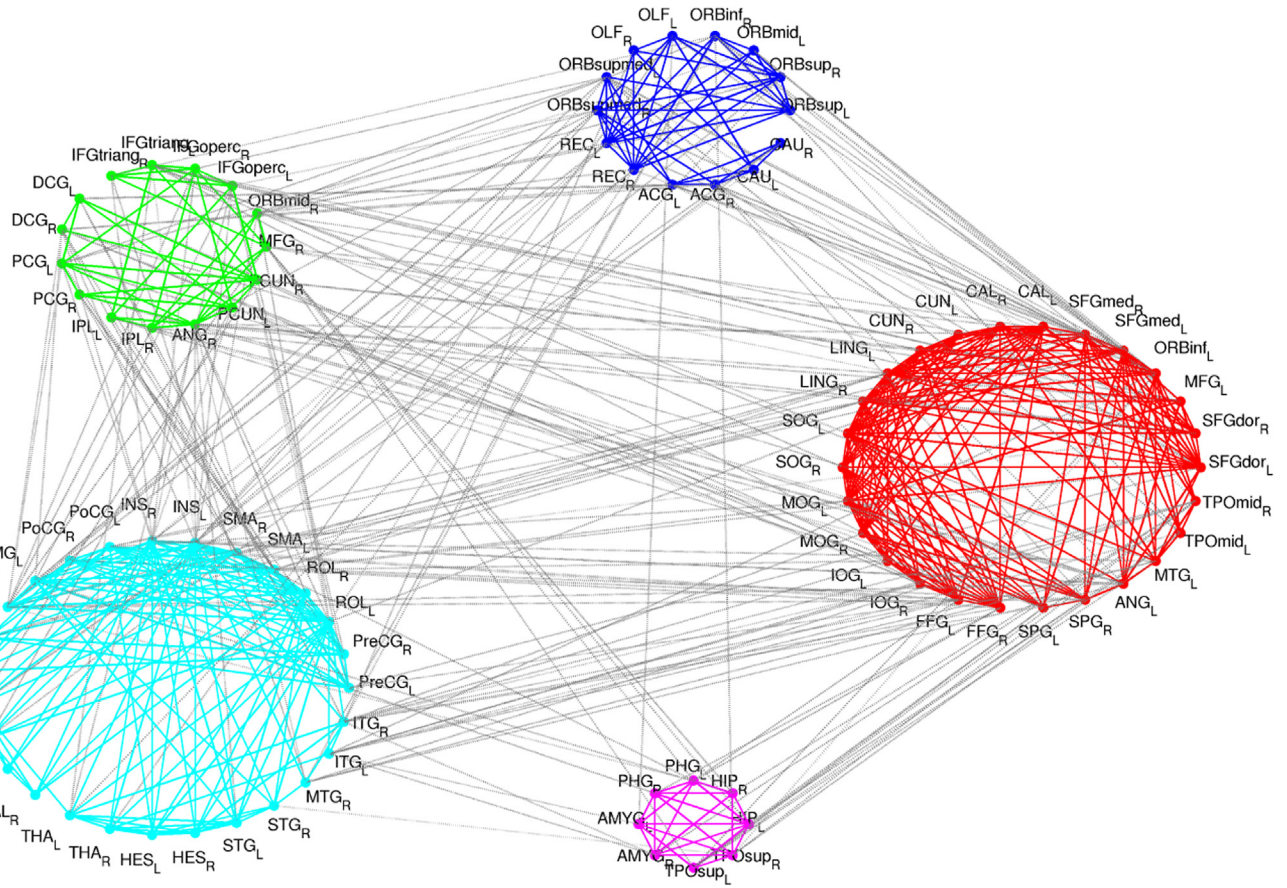


**Fig. 5.** Anatomical representation of the modularity analysis for the group-based connectivity network in the APTD condition at wiring cost  $K = 0.15$ . Nodes in each of the 5 modules and edges within them are plotted with a single color, while edges between modules are plotted in black. Comparison with Fig. 4 shows that dopamine depletion changes the modularity structure in the functional network. The basal ganglia module present in the BAL condition (magenta color in Fig. 4) is no longer evident in this dopamine depletion condition, while the separate auditory (green in Fig. 4) and sensorimotor (cyan in Fig. 4) modules are now grouped as one (cyan here). (For interpretation of the references to color in this figure legend, the reader is referred to the web version of this article.)

dopamine levels and stimulated (phasic) dopamine release in humans (Montgomery et al., 2003; Leyton et al., 2004). It is estimated that the reduction in tonic striatal dopamine is on the order of 10–20% (Montgomery et al., 2003) while the reduction in phasic dopamine is approximately 30% (McTavish et al., 1999b; Leyton et al., 2004). The treatment impairs performance on tasks dependent on frontal lobe function and working memory (Harmer et al., 2001; Gijnsman et al., 2002; Harrison et al., 2004) to a degree that correlates with the level of striatal dopamine depletion as measured by positron emission tomography (Mehta et al., 2005). Though dopamine is also a precursor for norepinephrine, accumulating microdialysis, cFos, and neuroendocrine studies suggest that APTD does not decrease norepinephrine neurotransmission (Sheehan et al., 1996; McTavish et al., 1999b, 1999a; Masurier et al., 2004).

The correlation analysis showed that dopamine precursor depletion increased functional connectivity between regions included in the DMN and those associated with the TPN. For example, during APTD, the PCC, a DMN region, was reassigned to a module that included the TPN regions dorsolateral and ventrolateral prefrontal cortex (Fig. 5). In addition, we found that the lowered dopamine state reduced connections within the TPN, most notably affecting the frontal lobes. DMN and TPN are typically anti-correlated (Fox et al., 2009, 2005), both at rest and during cognitive tasks, and the degree of anti-correlation appears to predict aspects of task performance (Kelly et al., 2008). The reduced segregation of

TPN and DMN regions seen here during APTD, and the reduced intra-TPN connectivity, may account for cognitive or attentional deficits in states of low dopamine transmission. Consistent with this interpretation, Kelly et al. (2009) reported that L-dopa, a dopamine precursor, reduced resting state functional connectivity between the striatum and regions associated with the DMN, while increasing connectivity between striatum and TPN. Dang et al. (2012a,b) recently demonstrated that this “anti-coupling” was dependent on intrinsic dopamine synthetic activity as measured by [ $^{18}\text{F}$ ]Fluoro-L-m-Tyrosine positron emission tomography. Similarly, we previously showed that APTD led to reduced frontal (TPN) – striatal connectivity and impaired DMN deactivation during performance of the Wisconsin Card Sorting task (Nagano-Saito et al., 2008). This has implications for cognitive deficits in diseases associated with impaired dopamine signaling: poor DMN deactivation or impaired TPN/DMN segregation is described in Parkinson’s disease (Delaveau et al., 2010), attention deficit hyperactivity disorder (Castellanos et al., 2008), and schizophrenia (Whitfield-Gabrieli et al., 2009). All these results point to a role of dopamine in maintaining segregation of the TPN and DMN during cognitive tasks, possibly via an influence on the striatum, which has extensive anatomical connections to both TPN and DMN. Further supporting a striatal locus for this effect of dopamine is a recent study showing that homozygous carriers of the 10-repeat allele of the dopamine transporter DAT1 demonstrate impaired TPN-DMN segregation at rest compared to 9-allele carriers (Gordon et al.,

2012). 10/10 homozygotes have lower tonic dopamine levels in the striatum. This is also consistent with our finding that APTD disperses the striatal module.

It is also possible that the previously observed inter-individual variability in this anti-correlation (Kelly et al., 2008) is a reflection of dopaminergic neurotransmission, which also shows inter-individual variability (e.g. Gordon et al., 2012). More generally, the proposed flexible coupling of TPN, DMN, and dorsal attentional modules as a function task requirements (Spreng et al., 2010) may also be under dopaminergic control.

Consistent with a role for dopamine in segregating functional networks during task performance, we also found a reduction in modularity in the low dopamine state. High modularity values imply that the within-module connections are greater than in an equivalent random network. Our analysis of the group-based networks disclosed a modular organization similar to that obtained by Meunier et al. (2009) and He et al. (2009b). Although the reduction in the number of modules in APTD only showed a trend towards statistical significance, we observed an effect of dopamine on the distribution of modules. In particular, APTD appeared to disrupt the organization of the striatal and limbic modules, which receive the greatest dopamine innervation of any brain region. Modularity is an intrinsic feature of small-world networks (Meunier et al., 2009), and likely underpins parallel information processing.

We also found significantly greater global and local efficiency for BAL relative to APTD, which shows that dopamine precursor depletion impairs the low-cost high-efficiency arrangement of brain functional networks. Our results are consistent with those of Achard and Bullmore (2007), who showed that a single dose of sulpiride, a dopamine antagonist, also impairs efficiency in brain functional networks.

Finally, dopamine precursor depletion reduced the regional efficiency of a number of limbic and paralimbic regions, namely orbitofrontal cortex and amygdala. This implies that connections between these regions, which receive significant dopaminergic innervation, and the rest of the brain were made less efficient by dopamine depletion.

These findings demonstrate that dopamine plays a role in the large-scale coordination of efficient brain network function. This may account in part for the cognitive impairment that accompanies dopaminergic dysfunction in conditions like Parkinson's disease, attention deficit hyperactivity disorder, and schizophrenia.

#### 4.2. Methodological considerations

We used a fairly simple approach to generate graphs based on pairwise correlations within the resting state BOLD time series. Since anti-correlations between regions also imply a form of mutual influence and may reasonably be used in graph generation (Fornito et al., 2013), we chose not to make distinction between positive and negative correlations. That is, we took the absolute correlation value to generate our graphs, a not uncommon approach (Achard et al., 2006; Achard and Bullmore, 2007). In any case, the top panels of Fig. 1 demonstrate that there were no statistically significant anti-correlations in our dataset. It is also worth mentioning that the global average signal (Fox et al., 2005) was not included as a confounding variable in our analysis. It is a matter of ongoing debate whether resting state anti-correlations are a measure of intrinsic slow fluctuations of brain activity or mostly spurious correlations introduced by removing the global average signal (Murphy et al., 2009; Fox et al., 2009). While global average signal removal may introduce false positive anti-correlations, failure to do so could obscure true correlations of neural origin (Chang and Glover, 2009). Since we do not know the effect of our dopaminergic manipulations on global resting state fluctuations, we

considered it prudent not to include the global average signal in our model. We attempted to control for physiological noise using the CORSICA algorithm and by including WM and CSF time-courses as confounds. The dopaminergic effects on DMN and TPN functional connectivity may represent reduced anti-correlation between these two sets of region in the lowered dopamine state, but these results should be interpreted with caution.

The choice of a suitable statistical model for the error term in fMRI signals is also of particular importance for estimating functional connectivity in resting state studies (Lund et al., 2006). Typical resting state fMRI time series have a slowly decaying autocorrelation structure (long memory processes). Whitening serially correlated data is the most efficient approach prior to estimating correlation parameters (Friston et al., 2000). Several models and whitening strategies have been proposed. For instance, the so-called 1/f model (Zarahn et al., 1997; Achard et al., 2006; Achard and Bullmore, 2007) assumes that the spectral density function of resting state fMRI BOLD signals behaves like the function 1/f. Under this assumption, wavelets filters have been used to decorrelate time series and a wavelets correlation coefficient (Percival and Walden, 2000) has been defined to estimate functional connectivity (Achard et al., 2006; Achard and Bullmore, 2007). The wavelets correlation coefficient provides a scale by scale decomposition of the usual correlation coefficient between time series. Hence, it allows focusing on the functional connectivity between brain regions with underlying activity in a pre-defined frequency interval or wavelet scale (Achard and Bullmore, 2007). However, the wavelets correlation coefficient is a relatively new concept and its distributional properties have not been fully studied (see Appendix A in Achard et al., 2006). Evidently, this limitation constrains useful classical inferential procedures over samples of independent correlation coefficients (i.e. group-based correlation coefficients analysis). Another general class of models for noise in fMRI time series is given by the  $AR(p)$  process, where  $p$  denotes the order of the auto-regressive model (Bullmore et al., 1996; Worsley et al., 2002; Penny et al., 2003). A detailed comparison between both types of model was carried out in Friston et al. (2000), where it was shown that low order  $AR(p)$  models fail to reproduce long range serial correlations (i.e. low frequency oscillations). On the other hand, it was also shown that the 1/f model is a good approximation for intermediate correlations but fails to model the long-range correlations as well as a high order  $AR(p)$  (Friston et al., 2000). In this work, we used an  $AR(8)$  model for describing the intrinsic autocorrelation structure in our fMRI data. This choice was based on the observations that the last AR coefficient was very close to zero for all data samples. Indeed, the last AR coefficient in a  $AR(p)$  model is called  $p$ th partial autocorrelation coefficient and measures the excess correlation at lag  $p$  which is not accounted by an  $AR(p - 1)$  model (Chatfield, 2004). A value of the  $p$ th partial autocorrelation coefficient close to zero is a good indicator that  $p$  is a correct order for modeling temporal autocorrelation. More precisely, values inside the range  $\pm 2/\sqrt{T}$  are not significantly different from zero at the  $\alpha = 0.05$  level, where  $T$  denotes the number of time instants. Here, we estimated partial autocorrelation coefficients by fitting  $AR(p)$  processes of successively higher order  $p$ , with  $p$  varying from 1 to 16. We verified that for all data samples the partial autocorrelation coefficients beyond  $p = 8$  were not significantly different from zero.

Another important issue when describing functional connectivity is the thresholding step. Individual and group-based correlation matrices need to be thresholded to generate the adjacency matrices that define the functional networks. Two different thresholding approaches have been used. The first approach, used here, sets the same cost threshold value  $0 < K < 1$  for all individual connectivity networks. This normalizes each individual network

with respect to the number of nodes and edges and allows an examination of relative network efficiency (He et al., 2009a), while limiting the number of spurious links at a group level. However, this approach risks allowing spurious (false positive) network connections. For instance, at an equal cost value, an overall reduction in correlation values would produce a higher proportion of spurious edges in the lower correlation network than in the higher correlation network. To overcome this limitation, a second thresholding strategy has been also used. Here all individual correlation matrices are thresholded at the same correlation value  $0 < r < 1$  (Achard et al., 2006). A conservative correlation threshold  $r$  close to 1 generates a sparse connectivity network structure, where the significant links should be interpreted as the strongest ones in the network. On the other hand, values of  $r$  close to 0 lead to densely connected networks, with a considerable number of spurious links. This thresholding approach allows the determination of absolute efficiency in each individual network, which is amenable to further statistical comparison between subjects and across groups. **Supplementary Figs. 1 and 2** show the effect of this second thresholding approach on our data. **Supplementary Fig. 1** shows, for both conditions, the average (across subjects) wiring cost values as a function of the correlation threshold  $r$ . Although not statistically significant different, the wiring cost values are greater in the APTD condition than in the BAL condition. This figure also shows the integrated (in the interval  $[0, 1]$ ) wiring cost contribution of our six pre-defined modules (see **Supplementary Table 1**) as well as their interactions. Notice that the wiring cost contribution to the interaction of these 6 modules does not significantly change across dopaminergic condition. **Supplementary Fig. 2** shows, for both conditions, the average (across subjects) global and local efficiency as a function of the correlation value. As for the cost-thresholded networks, there is statistically greater global and local efficiency during BAL than APTD for correlation values within the small-world range. The results showed in these two supplementary figures confirm that our findings in this paper do not depend on chosen thresholding approach.

## Acknowledgments

Supported by a Center of Excellence in Commercialization and Research (CECR) grant from Industry Canada, and by the Canadian Institutes for Health Research. FC was supported by a CECR fellowship.

## Appendix A. Supplementary data

Supplementary data related to this article can be found at <http://dx.doi.org/10.1016/j.neuropharm.2013.12.021>.

## References

- Achard, S., Bullmore, E., 2007. Efficiency and cost of economical brain functional networks. *PLoS Comput. Biol.* 3 (2), e17.
- Achard, S., Salvador, R., Whitcher, B., Suckling, J., Bullmore, E., 2006. A resilient, low-frequency, small-world human brain functional network with highly connected association cortical hubs. *J. Neurosci.* 26 (1), 63–72.
- Beckmann, C.F., DeLuca, M., Devlin, J.T., Smith, S.M., 2005. Investigations into resting-state connectivity using independent component analysis. *Phil. Trans. R. Soc. B Biol. Sci.* 360 (1457), 1001–1013.
- Bellec, P., Lavoie-Courchesne, S., Dickinson, P., Lerch, J.P., Zijdenbos, A.P., Evans, A.C., 2012. The pipeline system for Octave and Matlab (PSOM): a lightweight scripting framework and execution engine for scientific workflows. *Front. Neuroinform.* 6, 7.
- Bellec, P., Rosa-Neto, P., Lyttelton, O.C., Benali, H., Evans, A.C., 2010. Multi-level bootstrap analysis of stable cluster in resting-state fMRI. *NeuroImage* 51, 1126–1139.
- Benjamini, Y., Yekutieli, D., 2001. The control of the false discovery rate in multiple testing under dependency. *Ann. Stat.* 29 (4), 1165–1188.

- Biswal, B., Yetkin, F.Z., Haughton, V.M., Hyde, J.S., 1995. Functional connectivity in the motor cortex of resting human brain using echo-planar MRI. *Mag. Reson. Med.* 34 (4), 537–541.
- Bullmore, E., Brammer, M., Williams, S.C.R., Rabe-Hesketh, S., Janot, N., David, A., Mellers, J., Howard, R., Sham, P., 1996. Statistical methods of estimation and inference for functional MR image analysis. *Mag. Reson. Med.* 35 (2), 261–277.
- Bullmore, E., Sporns, O., 2009. Complex brain networks: graph theoretical analysis of structural and functional systems. *Nat. Rev. Neurosci.* 10 (3), 186–198.
- Castellanos, F.X., Margulies, D.S., Kelly, C., Uddin, L.Q., Ghaffari, M., Kirsch, A., Shaw, D., Shehzad, Z., Di Martino, A., Biswal, B., Sonuga-Barke, E.J., Rotrosen, J., Adler, L.A., Milham, M.P., 2008. Cingulate-precuneus interactions: a new locus of dysfunction in adult attention-deficit/hyperactivity disorder. *Biol. Psychiatry* 63, 332–337.
- Chang, C., Glover, G., 2009. Effects of model-based physiological noise correction on default mode network anti-correlations and correlations. *NeuroImage* 47 (4), 1448–1459.
- Chatfield, C., 2004. *The Analysis of Time Series: an Introduction*, sixth ed. Chapman & Hall/CRC.
- Collins, D.L., Neelin, P., Peters, T.M., Evans, A.C., 1994. Automatic 3D intersubject registration of MR volumetric data in standardized Talairach space. *J. Comput. Assist. Tomogr.* 18 (2), 192–205.
- Cordes, D., Haughton, V.M., Arfanakis, K., Carew, J.D., Turski, P.A., Moritz, C.H., Quigley, M.A., Meyerand, M.E., 2001. Frequencies contributing to functional connectivity in the cerebral cortex in resting-state data. *Am. J. Neuroradiol.* 22 (7), 1326–1333.
- Costa, R.M., Lin, S.C., Sotnikova, T.D., Cyr, M., Gainetdinov, R.R., Caron, M.G., Nicoletis, M.A.L., 2006. Rapid alterations in corticostriatal ensemble coordination during acute dopamine-dependent motor dysfunction. *Neuron* 52 (2), 359–369.
- Coull, J.T., Hwang, H., Leyton, M., Dagher, A., 2012. Dopamine precursor depletion impairs timing in healthy volunteers by attenuating activity in putamen and SMA. *J. Neurosci.* 32 (47), 16704–16715.
- Dang, L.C., O'Neil, J.P., Jagust, W.J., 2012a. Dopamine supports coupling of attention-related networks. *J. Neurosci.* 32, 9582–9587.
- Dang, L.C., Donde, A., Madison, C., O'Neil, J.P., Jagust, W.J., 2012b. Striatal dopamine influences the default mode network to affect shifting between object features. *J. Cog. Neurosci.* 24, 1960–1970.
- Delaveau, P., Salgado-Pineda, P., Fossati, P., Witjas, T., Azulay, J.P., Blin, O., 2010. Dopaminergic modulation of the default mode network in Parkinson's disease. *Eur. Neuropsychopharmacol.* 20, 784–792.
- De Luca, M., Beckmann, C.F., De Stefano, N., Matthews, P.M., Smith, S.M., 2006. fMRI resting state networks define distinct modes of long-distance interactions in the human brain. *NeuroImage* 29 (4), 1359–1367.
- Field, A.P., 2001. Meta-analysis of correlation coefficients: a Monte Carlo comparison of fixed-and random-effects methods. *Psychol. Methods* 6 (2), 161–180.
- Fortunato, S., 2010. Community detection in graphs. *Phys. Reports* 486, 75–184.
- Fornito, A., Zalesky, A., Breakspear, M., 2013. Graph analysis of the human connectome: promise, progress, and pitfalls. *NeuroImage* 80, 426–444.
- Fox, M.D., Snyder, A.Z., Vincent, J.L., Corbetta, M., Van Essen, D.C., Raichle, M.E., 2005. The human brain is intrinsically organized into dynamic, anticorrelated functional networks. *Proc. Natl. Acad. Sci.* 102 (27), 9673–9678.
- Fox, M.D., Corbetta, M., Snyder, A.Z., Vincent, J.L., Raichle, M.E., 2006. Spontaneous neuronal activity distinguishes human dorsal and ventral attention systems. *Proc. Natl. Acad. Sci.* 103 (26), 10046–10051.
- Fox, M.D., Raichle, M.E., 2007. Spontaneous fluctuations in brain activity observed with functional magnetic resonance imaging. *Nat. Rev. Neurosci.* 8 (9), 700–711.
- Fox, M.D., Zhang, D., Snyder, A.Z., Raichle, M.E., 2009. The global signal and observed anticorrelated resting state brain networks. *J. Neurophysiol.* 101 (6), 3270–3283.
- Freeman, L.C., 1977. A set of measures of centrality based on betweenness. *Sociometry* 40 (1), 35–41.
- Friston, K.J., Josephs, O., Zarahn, E., Holmes, A.P., Rounette, S., Poline, J.B., 2000. To smooth or not to smooth? Bias and efficiency in fMRI time-series analysis. *NeuroImage* 12 (2), 196–208.
- Gijsman, H.J., Scarna, A., Harmer, C.J., McTavish, S.F.B., Odontiadis, J., Cowen, P.J., Goodwin, G.M., 2002. A dose-finding study on the effects of branch chain amino acids on surrogate markers of brain dopamine function. *Psychopharmacologia* 160 (2), 192–197.
- Good, B.H., de Montjoye, Y.A., Clauset, A., 2010. The performance of modularity maximization in practical contexts. *Phys. Rev. E* 81 (4), 046106.
- Gordon, E.M., Stollstorff, M., Devaney, J.M., Bean, S., Vaidya, C.J., 2012. Effect of dopamine transporter genotype on intrinsic functional connectivity depends on cognitive state. *Cereb. Cortex* 22, 2182–2196.
- Greicius, M.D., Krasnow, B., Reiss, A.L., Menon, V., 2003. Functional connectivity in the resting brain: a network analysis of the default mode hypothesis. *Proc. Natl. Acad. Sci.* 100 (1), 253–258.
- Harmer, C.J., McTavish, S.F.B., Clark, L., Goodwin, G.M., Cowen, P.J., 2001. Tyrosine depletion attenuates dopamine function in healthy volunteers. *Psychopharmacologia* 154 (1), 105–111.
- Harrison, B.J., Olver, J.S., Norman, T.R., Burrows, G.D., Wesnes, K.A., Nathan, P.J., 2004. Selective effects of acute serotonin and catecholamine depletion on memory in healthy women. *J. Psychopharmacol.* 18 (1), 32–40.
- He, Y., Dagher, A., Chen, Z., Charil, A., Zijdenbos, A.P., Worsley, K.J., Evans, A.C., 2009a. Impaired small-world efficiency in structural cortical networks in

- multiple sclerosis associated with white matter lesion load. *Brain* 132 (12), 3366–3379.
- He, Y., Wang, J., Wang, L., Chen, Z.J., Yan, C., Yang, H., Tang, H., Zhu, C., Gong, Q., Zang, Y., Evans, A.C., 2009b. Uncovering intrinsic modular organization of spontaneous brain activity in humans. *PLoS ONE* 4 (4), e5226.
- Helmich, R.C., Derikx, L.C., Bakker, M., Scheeringa, R., Bloem, B.R., Toni, I., 2010. Spatial remapping of cortico-striatal connectivity in Parkinson's disease. *Cereb. Cortex* 20 (5), 1175–1186.
- Honey, G.D., Bullmore, E., 2004. Human pharmacological MRI. *Trends Pharmacol. Sci.* 25 (7), 366–374.
- Honey, G.D., Suckling, J., Zelaya, F., Long, C., Routledge, C., Jackson, S., Ng, V., Fletcher, P.C., Williams, S.C.R., Brown, J., Bullmore, E., 2003. Dopaminergic drug effects on physiological connectivity in a human cortico-striato-thalamic system. *Brain* 126 (8), 1767–1781.
- Karrer, B., Levina, E., Newman, M.E.J., 2008. Robustness of community structure in networks. *Phys. Rev. E* 77, 046119.
- Kelly, A.M.C., de Zubicaray, G., Gee, D., Shehzad, Z., Gotimer, K., Di Martino, A., Copland, D., Klein, D.F., Adler, L., Rotrosen, J., Castellanos, F.X., McMahon, K., Milham, M.P., 2009a. Is there an inverted U-shaped relationship between dopamine levels and resting state functional connectivity? *NeuroImage* 47 (Suppl. 1), S60.
- Kelly, A.M.C., Uddin, L.Q., Biswal, B.B., Castellanos, F.X., Milham, M.P., 2008. Competition between functional brain networks mediates behavioral variability. *NeuroImage* 39 (1), 527–537.
- Kelly, A.M.C., de Zubicaray, G., Di Martino, A., Copland, D., Reiss, P.T., Klein, D.F., Castellanos, F.X., Milham, M.P., McMahon, K., 2009. L-dopa modulates functional connectivity in striatal cognitive and motor networks: a double-blind placebo-controlled study. *J. Neurosci.* 29 (22), 7364–7378.
- Kiviniemi, V., Kantola, J.H., Jauhiainen, J., Hyvarinen, A., Tervonen, O., 2003. Independent component analysis of nondeterministic fMRI signal sources. *NeuroImage* 19 (2), 253–260.
- Latora, V., Marchiori, M., 2001. Efficient behavior of small-world networks. *Phys. Rev. Lett.* 87 (19), 198701.
- Leyton, M., Dagher, A., Boileau, I., Casey, K., Baker, G.B., Diksic, M., Gunn, R., Young, S.N., Benkelfat, C., 2004. Decreasing amphetamine-induced dopamine release by acute phenylalanine/tyrosine depletion: a PET/[11] raclopride study in healthy men. *Neuropsychopharmacology* 29 (2), 427–432.
- Leyton, M., Young, S.N., Pihl, R.O., Etezadi, S., Lauze, C., Blier, P., Baker, G.B., Benkelfat, C., 2000. Effects on mood of acute phenylalanine/tyrosine depletion in healthy women. *Neuropsychopharmacology* 22 (1), 52–63.
- Liu, Y., Liang, M., Zhou, Y., He, Y., Hao, Y., Song, M., Yu, C., Liu, H., Liu, Z., Jiang, T., 2008. Disrupted small-world networks in schizophrenia. *Brain* 131 (4), 945–961.
- Lowe, M.J., Mock, B.J., Sorenson, J.A., 1998. Functional connectivity in single and multislice echoplanar imaging using resting-state fluctuations. *NeuroImage* 7 (2), 119–132.
- Lund, T.E., Madsen, K.H., Sidaros, K., Luo, W.L., Nichols, T.E., 2006. Non-white noise in fMRI: does modelling have an impact? *NeuroImage* 29 (1), 54–66.
- Maslov, S., Sneppen, K., 2002. Specificity and stability in topology of protein networks. *Science* 296, 910–913.
- Masurier, M.L., Cowen, P.J., Sharp, T., 2004. Fos immunocytochemical studies on the neuroanatomical sites of action of acute tyrosine depletion in the rat brain. *Psychopharmacology* 171 (4), 435–440.
- McTavish, S., Callado, L., Cowen, P., Sharp, T., 1999a. Comparison of the effects of  $\alpha$ -methyl-p-tyrosine and a tyrosine-free amino acid load on extracellular noradrenaline in the rat hippocampus in vivo. *J. Psychopharmacol.* 13 (4), 379–384.
- McTavish, S.F.B., Cowen, P.J., Sharp, T., 1999b. Effect of a tyrosine-free amino acid mixture on regional brain catecholamine synthesis and release. *Psychopharmacology* 141 (2), 182–188.
- Mehta, M.A., Gumaste, D., Montgomery, A.J., McTavish, S.F.B., Grasby, P.M., 2005. The effects of acute tyrosine and phenylalanine depletion on spatial working memory and planning in healthy volunteers are predicted by changes in striatal dopamine levels. *Psychopharmacology* 180 (4), 654–663.
- Meunier, D., Achard, S., Morcom, A., Bullmore, E., 2009. Age-related changes in modular organization of human brain functional networks. *NeuroImage* 44 (3), 715–723.
- Meyer-Lindenberg, A., Straub, R.E., Lipska, B.K., Verchinski, B.A., Goldberg, T., Callicott, J.H., Egan, M.F., Huffaker, S.S., Mattay, V.S., Kolachana, B., et al., 2007. Genetic evidence implicating DARPP-32 in human frontostriatal structure, function, and cognition. *J. Clin. Investig.* 117 (3), 672–682.
- Montgomery, A.J., McTavish, S.F.B., Cowen, P.J., Grasby, P.M., 2003. Reduction of brain dopamine concentration with dietary tyrosine plus phenylalanine depletion: an [11C] raclopride PET study. *Am. J. Psychiatry* 160 (10), 1887–1889.
- Murphy, K., Birn, R.M., Handwerker, D.A., Jones, T.B., Bandettini, P.A., 2009. The impact of global signal regression on resting state correlations: are anti-correlated networks introduced? *NeuroImage* 44 (3), 893–905.
- Nagano-Saito, A., Leyton, M., Monchi, O., Goldberg, Y.K., He, Y., Dagher, A., 2008. Dopamine depletion impairs frontostriatal functional connectivity during a set-shifting task. *J. Neurosci.* 28 (14), 3697–3706.
- Nagano-Saito, A., Cisek, P., Perna, A.S., Shirdel, F.Z., Benkelfat, C., Leyton, M., Dagher, A., 2012. From anticipation to action, the role of dopamine in perceptual decision-making: an fMRI – tyrosine depletion study. *J. Neurophysiol.* 108 (2), 501–512.
- Newman, M., Girvan, M., 2004. Finding and evaluating community structure in networks. *Phys. Rev. E* 69 (2), 26113.
- Newman, M., 2006. Modularity and community structure in networks. *PNAS* 103 (23), 8577–8582.
- Palmour, R.M., Ervin, F.R., Baker, G.B., Young, S.N., 1998. An amino acid mixture deficient in phenylalanine and tyrosine reduces cerebrospinal fluid catecholamine metabolites and alcohol consumption in vervet monkeys. *Psychopharmacology* 136 (1), 1–7.
- Penny, W., Kiebel, S., Friston, K.J., 2003. Variational Bayesian inference for fMRI time series. *NeuroImage* 19 (3), 727–741.
- Percival, D.B., Walden, A.T., 2000. *Wavelet Methods for Time Series Analysis*. Cambridge University Press.
- Perlberg, V., Bellec, P., Anton, J.L., Pelegrini-Issac, M., Doyon, J., Benali, H., 2007. CORSICA: correction of structured noise in fMRI by automatic identification of ICA components. *Magn. Reson. Imaging* 25 (1), 35–46.
- Pessiglione, M., Guehl, D., Rolland, A.S., Francois, C., Hirsch, E.C., Feger, J., Tremblay, L., 2005. Thalamic neuronal activity in dopamine-depleted primates: evidence for a loss of functional segregation within basal ganglia circuits. *J. Neurosci.* 25 (6), 1523–1531.
- Pinheiro, J.C., Bates, D.M., 2000. *Mixed-effects Models in S and S-PLUS*. Springer, New York.
- Raichle, M.E., MacLeod, A.M., Snyder, A.Z., Powers, W.J., Gusnard, D.A., Shulman, G.L., 2001. A default mode of brain function. *Proc. Natl. Acad. Sci. U.S.A.* 98, 676–682.
- Salvador, R., Suckling, J., Coleman, M.R., Pickard, J.D., Menon, D., Bullmore, E., 2005. Neurophysiological architecture of functional magnetic resonance images of human brain. *Cereb. Cortex* 15 (9), 1332–1342.
- Sheehan, B.D., Tharyan, P., McTavish, S.F.B., Campling, G.M., Cowen, P.J., 1996. Use of a dietary manipulation to deplete plasma tyrosine and phenylalanine in healthy subjects. *J. Psychopharmacol.* 10 (3), 231–234.
- Spreng, R.N., Stevens, W.D., Chamberlain, J.P., Gilmore, A.W., Schacter, D.L., 2010. Default network activity, coupled with the frontoparietal control network, supports goal-directed cognition. *NeuroImage* 53, 303–317.
- Supekar, K., Menon, V., Rubin, D., Musen, M., Greicius, M.D., 2008. Network analysis of intrinsic functional brain connectivity in Alzheimer's disease. *PLoS Comput. Biol.* 4 (6), e1000100.
- Tzourio-Mazoyer, N., Landeau, B., Papathanassiou, D., Crivello, F., Etard, O., Delcroix, N., Mazoyer, B., Joliot, M., 2002. Automated anatomical labeling of activations in SPM using a macroscopic anatomical parcellation of the MNI MRI single-subject brain. *NeuroImage* 15 (1), 273–289.
- Walters, J.R., Ruskin, D.N., Allers, K.A., Bergstrom, D.A., 2000. Pre- and postsynaptic aspects of dopamine-mediated transmission. *Trends Neurosci.* 23, 41–47.
- Watts, D.J., Strogatz, S.H., 1998. Collective dynamics of "small-world" networks. *Nature* 393, 440–442.
- Whitfield-Gabrieli, S., Thermenos, H.W., Milanovic, S., Tsuang, M.T., Faraone, S.V., McCarley, R.W., Shenton, M.E., Green, A.I., Nieto-Castanon, A., LaViolette, P., Wojcik, J., Gabrieli, J.D.E., Seidman, L.J., 2009. Hyperactivity and hyperconnectivity of the default network in schizophrenia and in first-degree relatives of persons with schizophrenia. *Proc. Natl. Acad. Sci.* 106, 1279–1284.
- Worsley, K.J., Liao, C.H., Aston, J., Petre, V., Duncan, G.H., Morales, F., Evans, A.C., 2002. A general statistical analysis for fMRI data. *NeuroImage* 15 (1), 1–15.
- Worsley, K.J., Taylor, J.E., Carbonell, F., Chung, M.K., Duerden, E., Bernhardt, B., Lyttelton, O., Boucher, M., Evans, A.C., 2009. SurfStat: a Matlab toolbox for the statistical analysis of univariate and multivariate surface and volumetric data using linear mixed effects models and random field theory. In: *Proceedings of the 15th Annual Meeting of the Organization for Human Brain Mapping*, San Francisco, CA, USA.
- Zarahn, E., Aguirre, G.K., D'Esposito, M., 1997. Empirical analysis of BOLD fMRI statistics. I. Spatially smoothed data collected under null-hypothesis and experimental conditions. *NeuroImage* 5, 179–197.
- Zijdenbos, A.P., Forghani, R., Evans, A.C., 2002. Automatic "pipeline" analysis of 3-D MRI data for clinical trials: application to multiple sclerosis. *IEEE Trans. Med. Imaging* 21 (10), 1280–1291.